UC Irvine

Title
Numerical study on wave-induced beam ion prompt losses in DIII-D tokamak

Permalink
https://escholarship.org/uc/item/5v15s083

Journal
Physics of Plasmas, 24(8)

ISSN
1070-664X

Authors
Feng, Zhichen
Zhu, Jia
Fu, Guo-Yong
et al.

Publication Date
2017-08-01

DOI
10.1063/1.5000073

Copyright Information

Peer reviewed

Numerical study on wave-induced beam ion prompt losses in DIII-D tokamak

Zhichen Feng,[1] Jia Zhu,[1] Guo-Yong Fu,[1,2,a)] W. W. Heidbrink,[3] and M. A. Van Zeeland[4]

[1]*Institute for Fusion Theory and Simulation and Department of Physics, Zhejiang University, Hangzhou 310027, China*
[2]*Princeton Plasma Physics Laboratory, Princeton, New Jersey 08543, USA*
[3]*Department of Physics and Astronomy, University of California Irvine, Irvine, California 92697, USA*
[4]*General Atomics, San Diego, California 92186, USA*

A numerical study is performed on the coherent beam ion prompt losses driven by Alfvén eigenmodes (AEs) in DIII-D plasmas using realistic parameters and beam ion deposition profiles. The synthetic signal of a fast-ion loss detector (FILD) is calculated for a single AE mode. The first harmonic of the calculated FILD signal is linearly proportional to the AE amplitude with the same AE frequency in agreement with the experimental measurement. The calculated second harmonic is proportional to the square of the first harmonic for typical AE amplitudes. The coefficient of quadratic scaling is found to be sensitive to the AE mode width. The second part of this work considers the AE drive due to coherent prompt loss. It is shown that the loss-induced mode drive is much smaller than the previous estimate and can be ignored for mode stability. *Published by AIP Publishing.* [http://dx.doi.org/10.1063/1.5000073]

I. INTRODUCTION

Coherent beam ion losses driven by Alfven eigenmodes (AEs) were recently observed in tokamak and stellarator plasmas heated by neutral beam injection.[1–9] The losses were measured using a Fast Ion Loss Detector (FILD) with a high frequency response and were coherent with the Alfvén eigenmodes. It was shown that the coherent losses in DIII-D mainly come from trapped particles whose orbits are close to the tokamak wall.[5,6] These trapped ions are first ionized close to the edge of the plasma, are "kicked out" radially by the Alfvén modes via wave particle interactions, and are then lost to the wall within one bounce of the banana orbits. The coherent FILD signals oscillate at the same frequencies of the corresponding AEs, while the amplitudes of the FILD signals are proportional to those of the AEs. These experimental results of AE-induced prompt losses have been explained successfully by an analytic theory as well as numerical simulation by Zhang *et al.*[10] It was shown that the AE induces a radial displacement of the banana orbit via the "local resonance" interaction[10] over the inner leg of the banana orbit which intersects the localized AE mode structure (see the orbit plotted in Fig. 1). The "local resonance" is also called "single-pass resonance" for particles which are lost after interacting with the AE mode in a single bounce orbit in some papers.[5,11] The calculated radial displacement (about a few centimeters) after one bounce is proportional to the AE amplitude with the same frequency. The local resonance condition is given by

$$\omega = n\langle\dot{\phi}\rangle - m\langle\dot{\theta}\rangle, \tag{1}$$

where ω is the AE mode frequency, n and m are the toroidal and poloidal mode numbers, and $\langle\dot{\phi}\rangle$ and $\langle\dot{\theta}\rangle$ are the

averaged toroidal and poloidal angular velocities over the part of the orbit which intersects with the localized AE mode. ϕ and θ are the straight field line toroidal and poloidal angle, respectively. The width of this local resonance is fairly large for the prompt-lost particles, on the order of several bounce frequencies, because the interaction time is shorter than one bounce period. These analytic results have been confirmed by numerical simulations and recent experimental results.[9]

In this work, a numerical study of AE-induced beam ion losses is performed using the realistic DIII-D experimental geometry, parameters, and profiles. First, we simulate the synthetic FILD signal of AE-induced losses for a single AE using the realistic neutral beam deposition profile from the
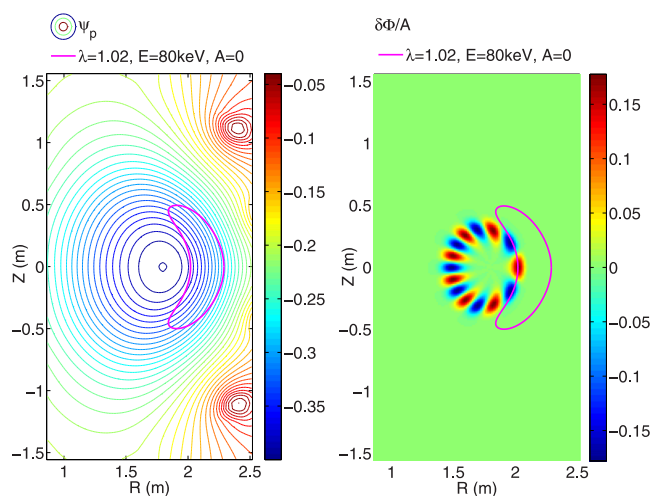

FIG. 1. Poloidal magnetic flux of DIII-D pulse 146 096 at 365 ms, given the perturbed AE electrostatic field normalized by the amplitude, and the equilibrium test particle orbit, where $\lambda = \mu B_0/E$ is the test particle's pitch angle. Only the inner leg of the banana orbit can interact with the localized AE mode.

a)Author to whom correspondence should be addressed: gyfu@zju.edu.cn

TRANSP code.[12] The energetic particle-Alfvén eigenmode code (EAC)[13] is adapted to simulate the fast ion interaction with AE, resultant losses, and associated FILD signals. Both the first and second harmonics of the FILD signal are calculated and compared with the experimental observation. This part of our work is mainly motivated by the recent experimental observation[9] where it was shown that the second harmonic has no clear correlation with the first harmonic. Here, the second harmonic of the FILD signal is calculated in order to explain this counter-intuitive observation. In the second part of our work, the AE drive due to AE-induced prompt loss is simulated. This is motivated by a recent work[11] where an order of magnitude estimate indicating the drive due to prompt loss can be significant. This work will give a more accurate evaluation of the drive using realistic parameters and beam ion deposition profiles. The EAC code is also used to compute the AE growth rate due to all prompt loss particles.

In Sec. II, the beam ion interaction with AE is studied for a model tokamak equilibrium and an analytic AE mode structure. In Secs. III and IV, the DIII-D FILD signal and contribution of prompt loss particles to AE mode drive are calculated at constant neutral beam injection power for realistic experimental parameters and profiles. Conclusions and discussions are given in Sec. V.

II. SIMULATION OF THE AE-INDUCED ENERGY CHANGE AFTER ONE BOUNCE

In this section, we calculate the energy change of trapped beam ions after the localized interaction within one bounce in order to compare with previous work and to understand the simulation results of AE-induced prompt losses shown in Sec. III. As will be shown later, the energy change is proportional to the radial displacement of the particle orbit. Therefore, the prompt loss is directly related to the particle energy change as a result of wave particle interactions. The calculation is done using the revised EAC code[13] where the guiding center equations in the EAC code are changed into the gyro-kinetic equations since the fast ion Larmor radius is comparable to the spatial scale of the AE mode structures.

Figure 1, left, shows the poloidal magnetic flux of DIII-D pulse 146096 at 365 ms and a typical trapped particle orbit close to the plasma edge at $R_{edge} = 2.30$ m. The wall is located at $R_{wall} = 2.363$ m. The major radius of the magnetic axis is $R_0 = 1.80$ m, and the toroidal magnetic field on the axis is $B_0 = 1.94$ T. Figure 1, right, shows the electrostatic potential of a prescribed Reversed Shear Alfven Eigenmode (RSAE) and a typical trapped particle orbit with its inner leg intersecting the localized AE mode structure. Figure 2 shows the reversed shear safety factor q profile at the outer midplane with the minimum value of about $q_{min} = 3.38$ at $R = 2.03$ m where the RSAE is localized. The equilibrium of DIII-D pulse 146096 at 365 ms is used throughout this paper except the cases where the q profile varies. In this work, we use both analytical RSAE mode structures and more realistic AE mode structures obtained from the NOVA code[14] based
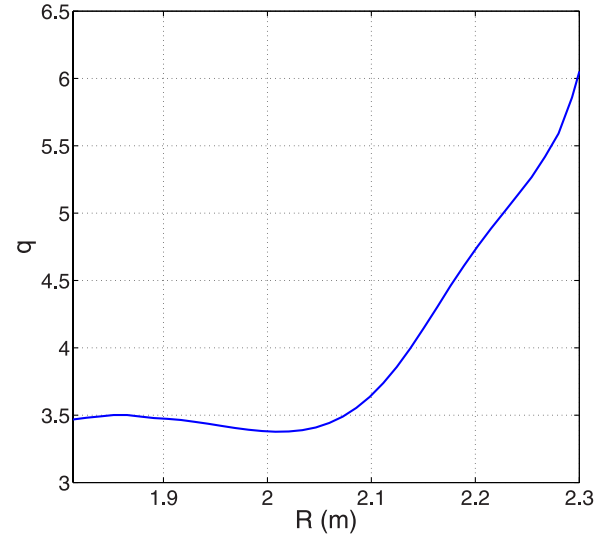

FIG. 2. Safety factor q profile in the outer midplane for the equilibrium of DIII-D pulse 146 096 at 365 ms.

on realistic equilibrium. The analytic RSAE mode structure, as shown in Fig. 1, is prescribed as

$$\delta\Phi = A\bar{\psi}_p \exp\left[-\left(\frac{\bar{\psi}_p - \bar{\psi}_{q_{min}}}{\Delta}\right)^2\right]\cos(-\omega t - (n\phi - m\theta)), \quad (2)$$

where A is the amplitude in Volts with the corresponding magnetic perturbation of $\delta B/B_0 \simeq 2 \times 10^{-7}$; $\bar{\psi}_p \equiv (\psi_p - \psi_{p_0})/(\psi_{edge} - \psi_{p_0})$ is the normalized poloidal magnetic flux, ψ_p, ψ_0, and ψ_{edge} are the poloidal magnetic flux at the grid point, the magnetic axis, and the plasma edge respectively, and $\bar{\psi}_{q_{min}}$ is the normalized poloidal magnetic flux at the minimum q surface; Δ is the normalized mode width; ω is the real frequency of the mode; ϕ is the toroidal angle, and θ is the straight field line poloidal angle; $n = 2$ and $m = 7$ are toroidal and poloidal mode numbers. This analytical mode structure is similar to the one used in the work by Zhang et al.[10] with $\Delta_0 \sim 0.1$ and $\omega_0 = 6.03 \times 10^5 \text{s}^{-1} (f_0 = 96 \text{ kHz})$.

Figure 3 shows the particle energy change after the banana orbit goes through the localized RSAE mode structure versus its initial toroidal angle for several mode amplitudes. The energy change is naturally a periodic function of the toroidal angle with the period being the same as the mode period (here, $2\pi/n = \pi$). The shape of the function is a distorted sine or cosine. The distortion is due to the nonlinear effect since the orbit changes as a result of particle interactions with the RSAE, which leads to the second harmonic of the energy change. The distortion becomes weak as the amplitude decreases as shown later. These results are similar to Zhang's work.

Figure 4 shows the test particles' energy change after one bounce versus the frequency of the given AE. Particles are initially distributed uniformly in $\phi \in [0, \pi]$. Like Zhang's work,[10] the resonance frequency width is quite large ($\sim 0.8\omega_0$), which is several bounce frequencies. There is a small second peak near $1.6\omega_0$, which may be a higher order local resonance. The envelop of the main peak is similar to Zhang's work.
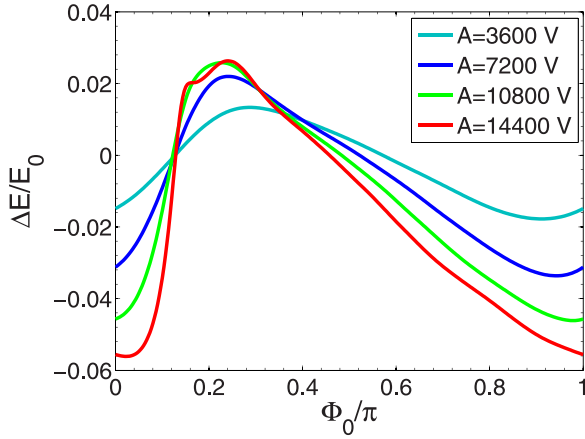
FIG. 3. Test particles' energy change after one bounce versus their initial toroidal angle for different amplitudes of AE modes, where $A = 10\,800$ V corresponds to $\delta B_{max}/B_0 = 0.002$.
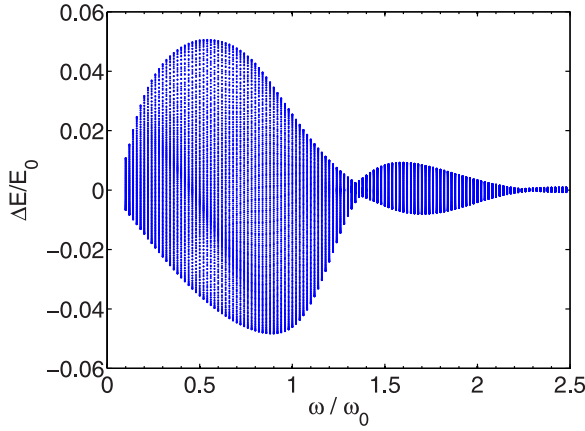

FIG. 4. Test particles' energy change after one bounce VS the frequency of given AEs. Particles are initially distributed uniformly in $\phi \in [0, \pi]$. Here, when $\omega/\omega_0 = 1$, $\delta B_{max} = 0.0045$ T, i.e., $\delta B_{max}/B_0 \approx 0.002$. δB_{max} will be proportional to ω_0/ω to keep $E_\parallel = 0$.

To examine the nonlinear dependence of the energy change on the wave amplitude, we carry out a Fourier analysis for curves shown in Fig. 3. Figure 5 plots the amplitudes and ratio of second and first harmonic of test particles' energy change versus wave amplitude. We observe that the ratio is almost linearly proportional to the wave amplitude in the low amplitude region.

Figure 6 shows the amplitudes and their ratio of δE second and first harmonics as a function of the mode width for particles initially located at $R = 2.26$ m and $Z = 0$ with $\lambda = 1.02$. This indicates that the size of the second harmonic is sensitive to the mode width.

The above results of test particle energy change due to one-bounce wave particle interactions can be used to understand the results in Sec. III for the simulated FILD signal because the energy change is directly related to the radial displacement of the test particles. According to the canonical Hamiltonian equations, the formula

$$\omega \dot{P}_\phi = n \dot{E}, \qquad (3)$$

always holds, provided that the given perturbation is a function of $(n\phi - \omega t)$ for a single mode in a tokamak,[15,16] where P_ϕ is the canonical toroidal momentum and E is the particle energy. Note that P_ϕ can be regarded as a radial variable. Thus, the energy change is proportional to the radial shift of the orbit, which indicates that the particles move in and out as a result of wave particle interaction. Since the radial shift is directly related to the FILD signal, the first and second harmonics of the energy change correspond to the first and second harmonics of the FILD signal.

III. FILD SIGNAL FROM NEUTRAL BEAM INJECTION

In this section, we simulate the FILD signal using realistic neutral beam deposition obtained from the TRANSP code[12] for the DIII-D discharge.

Figure 7 plots the DIII-D neutral beam deposition distribution for the 30L beamline in R-Z (on left) and X-Y (on right). Figure 8 plots the same deposition in the λ–P_ϕ phase space, where black, green, and blue lines correspond to prompt loss boundary of guiding centers, effective loss boundary due to the finite gyroradius, and trapped-passing boundary, respectively. The red points are the selected particles for our simulations. These are all trapped particles close to the plasma edge, whose orbits will intersect AE perturbation before they can be lost to the wall. The particles colored green in the loss and trapped region in Fig. 8 will be lost to the wall before they can interact with the AE and are thus not included in our simulations for saving computation time. The FILD's location $(R_{FILD}, Z_{FILD}, \phi_{FILD})$ is placed at the same point as it is in DIII-D shot 146096, where
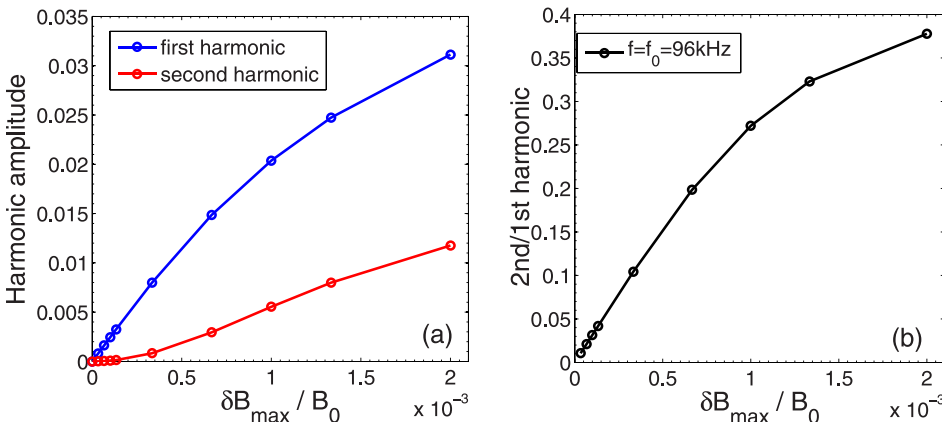

FIG. 5. Amplitudes of second and first harmonics (a) and their ratio (b) of test particles' energy change VS wave amplitude. The harmonics are the Fourier components of curves shown in Fig. 3 in one wave period.
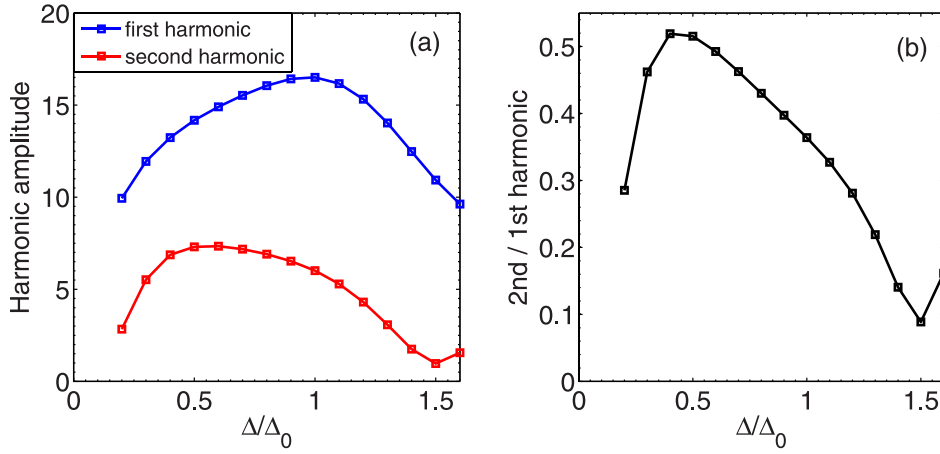
FIG. 6. (a) Amplitude of second and first harmonics and (b) their ratio of test particles' energy change VS wave width. Particles are initially located at $R = 2.26$ m and $Z = 0$ with $\lambda = 1.02$, uniformly distributed in $\phi \in [0, \pi]$.

$R_{FILD} = 2.36$ m, $Z_{FILD} = 0$, and $\phi_{FILD} = 4.974$ rad. To get a sufficiently large signal in numerical calculations, the FILD's window size is enlarged to ± 5 cm in Z and ± 0.1 rad around $\phi = \phi_{FILD}$.

We first calculate the FILD signal for a prescribed analytical AE structure of the $n = 2$ mode. In a wave period $T_p = 10^{-5}$ s, the FILD signal is calculated with continuous injection of the selected particles every two time steps, where the time step in our calculation is $\delta t = T_0/400 = 1/(400 f_0) = 2.604 \times 10^{-8}$ s. The injection lasts 5×10^{-5} s, which is about one bounce period of the selected particles. The results are shown in Fig. 9(a) for several mode amplitudes. As expected, the signal oscillates with the mode frequency after the initial transient phase. The signal tends to be constant when the wave amplitude is small (green curve), which corresponds to the intrinsic prompt loss signal from the 30L injected beam. The corresponding spectrum is plotted in Fig. 9(b) for several mode amplitudes. It should be noted that the FILD signal is exactly periodic since the AE perturbation has a single frequency. Therefore, the spectrum shown is discrete. Figure 10 plots the first and second harmonics of the FILD signal versus mode amplitude. It is clear that the size of the first harmonic is linearly proportional to

the mode amplitude when the mode amplitude is not too large, i.e., when $\delta B_{max}/B_0 < 0.001$.

Figure 11 plots the amplitude and ratio of the second harmonic and the first harmonic of the FILD signal versus the normalized mode width. We observe that the ratio is quite sensitive to the mode width and can vary about a factor of two from 0.1 to 0.2. Single particles' results shown in Fig. 6 lead to the complex behavior of the FILD signals' harmonics and their ratio. The sensitivity of the second harmonic to the mode width is presumably due to the complex nonlinearity of the local wave particle interaction. The results in Fig. 11 are consistent with the experimental observation[9] where the ratio is measured to be on the order of 0.1 and varies a lot.

We now simulate the FILD signal using the AE mode structure obtained from the NOVA code[14] in order to be more realistic in comparing the numerical FILD signals with experimental results. Fig. 12 shows the $n = 2$ AE frequencies and mode structures obtained using the NOVA code, where we vary the q profile by multiplying $q_{original}$ (the original q profile shown in Fig. 2) with a constant factor c so that $q = c q_{original}$. This factor is used to scan the value of q_{min} in a
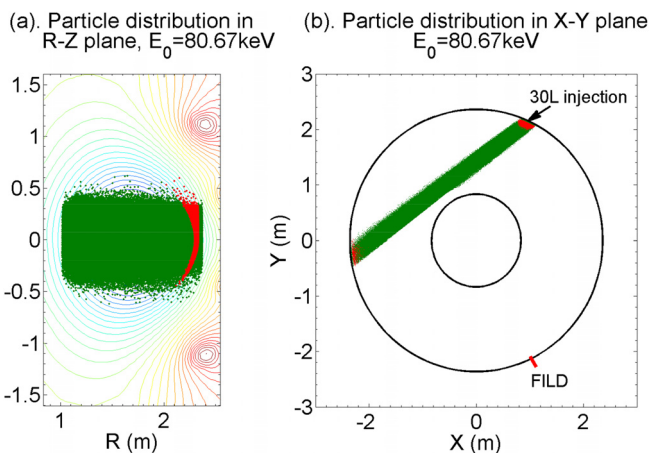

FIG. 7. DIII-D 30L neutral beam injection particle deposition (guiding center) distribution in (a) R-Z plane and (b) X-Y plane. The green points are the deposited particles. The red points are the particles used in our work to calculate the FILD signal and the loss particles' energy change.
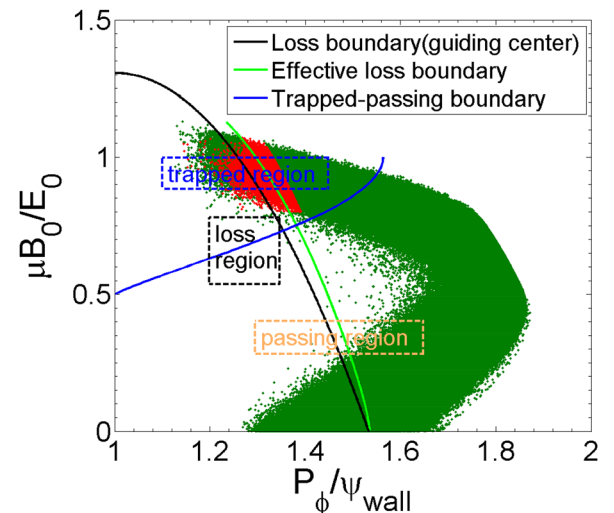

FIG. 8. DIII-D 30L neutral beam injection particle deposition (guiding center) distribution in the λ-P_ϕ plane, where $E_0 = 80.67$ keV. The effective boundary is the physical boundary minus the particle's Larmor radius.
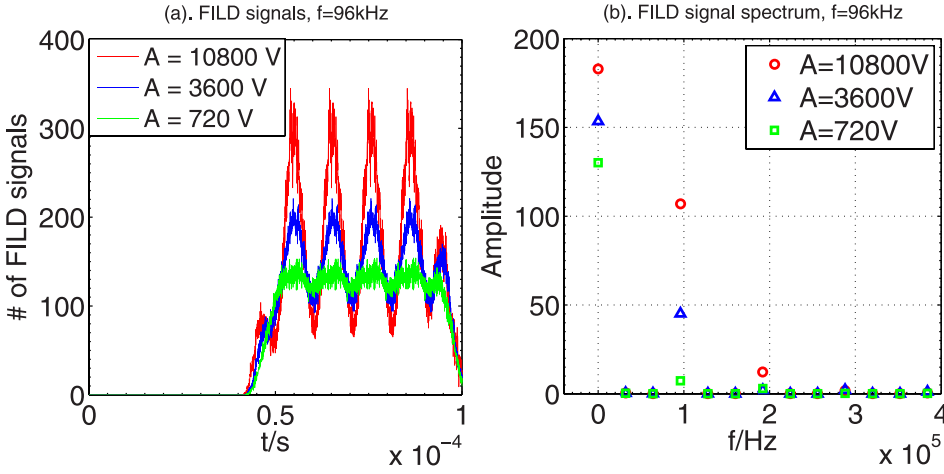
FIG. 9. (a) Real numerical FILD signals and (b) their spectrum. When $A = 10\,800$ V, $\delta B_{max}/B_0 \approx 0.002$, which is the same as the parameter in Fig. 3.
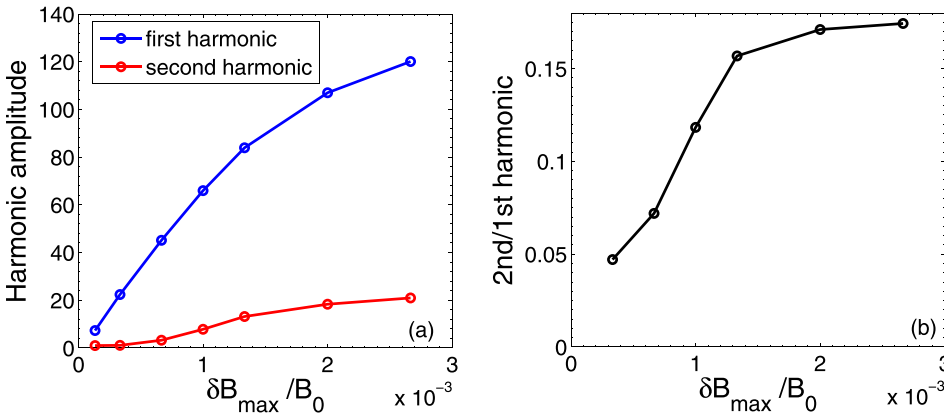

FIG. 10. (a) First and second harmonics amplitude of the FILD signal VS wave amplitude. (b)The ratio of the second harmonic over first harmonic VS wave amplitude.
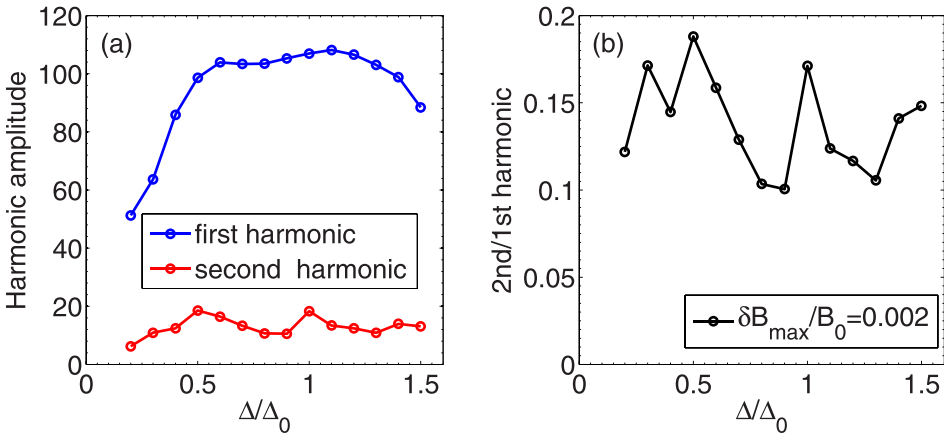

FIG. 11. (a) Amplitude and (b) ratio of 2nd and 1st harmonics of the FILD signal VS mode width, where $\Delta_0 = 0.1$ is the mode width defined after Eq. (2) on the normalized flux surface.

small range. As expected, when q_{min} becomes smaller, the sideband ($n = 2$ and $m = 6$ mode) of the n = 2 RSAE[17,18] increases and the mode frequency also increases. The RSAE eventually becomes a Toroidal Alfven Eigenmode (TAE)[19] at $q_{min} = 3.25$. NOVA results for n = 3 AE modes are similar as shown in Fig. 13.

The FILD signal is calculated for several mode amplitudes of $n = 2$ RSAE at $q = q_0$ [the corresponding $n = 2$ mode is shown in Fig. 12(a)]. Figure 14 plots the first and second harmonic amplitudes of the FILD signal and the ratio of second harmonic over first harmonic versus mode amplitude, respectively. In the low amplitude region in Figs. 10, 14 and 15, the amplitude of the first harmonic is almost linearly proportional to the mode amplitude, while the second

harmonic is approximately quadratic to the amplitude as long as the first harmonic is linear with regard to B_{max}/B_0 so that the ratio between them is linear to the wave amplitude. The results are similar for the $n = 3$ RSAE case plotted in Fig. 15.

Figure 16 plots the first and second harmonic as well as the ratio as a function of q_{min} for the $n = 2$ AE (see Fig. 12 for the corresponding mode structure and frequency at each $q(min)$). We observe that the absolute values and the ratio of these two harmonics change little when the q value is varied (the mode width remains almost the same when q varies). When RSAE changes to TAE as q_{min} decreases, the frequency of the AE increases about 20%, which tends to make the particles further from the local resonance peak shown in
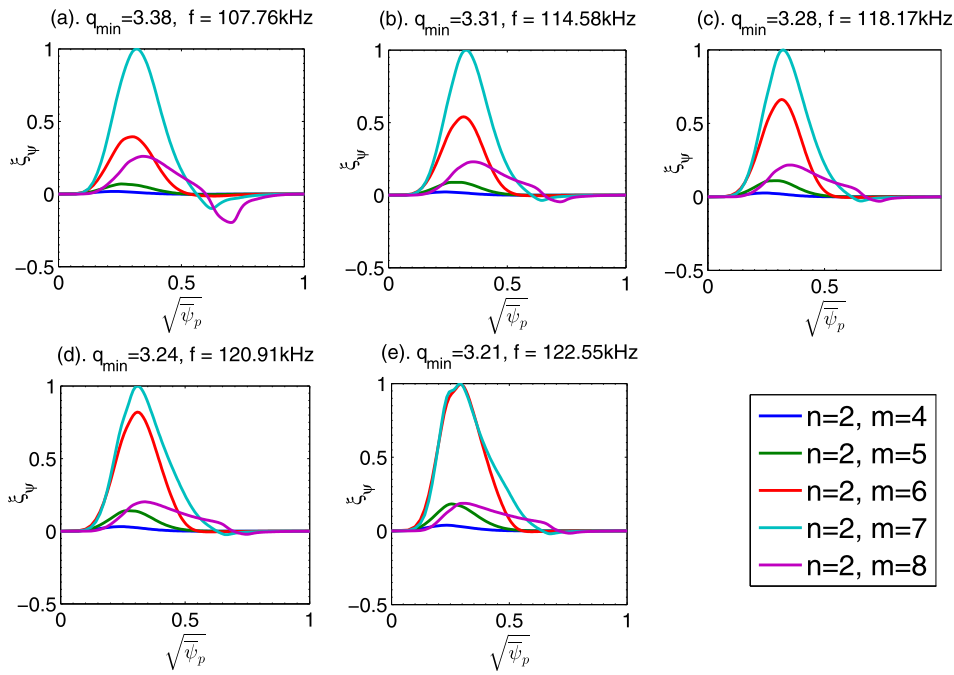
FIG. 12. $n=2$ AE frequencies and structures for different $q=cq_{original}$ values calculated using the NOVA code, where $q_{original}$ is the original q profile shown in Fig. 2, c is a constant factor modifying the q value to change q_{min}, ξ_ψ is defined by $\xi_\psi = \vec{\xi} \cdot \nabla \psi_p$, and $\vec{\xi}$ is the perturbed displacement vector.
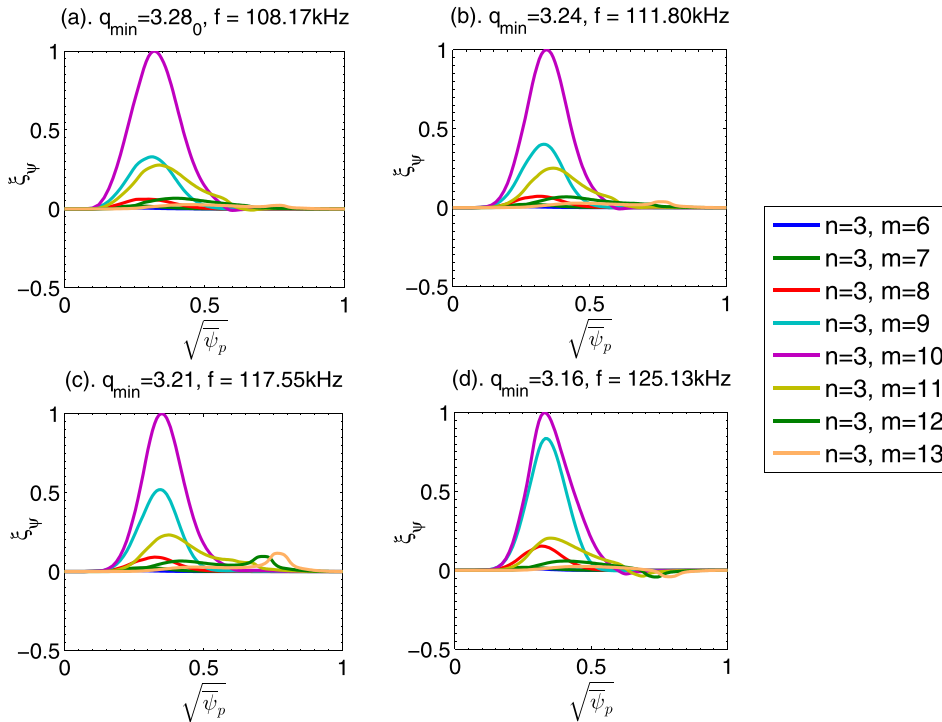

FIG. 13. $n=3$ AE frequencies and structures for different $q=cq_{original}$ values calculated using the NOVA code, where $q_{original}$ is the original q profile shown in Fig. 2, c is a constant factor modifying the q value to change q_{min}, ξ_ψ is defined by $\xi_\psi = \vec{\xi} \cdot \nabla \psi_p$, and $\vec{\xi}$ is the perturbed displacement vector.
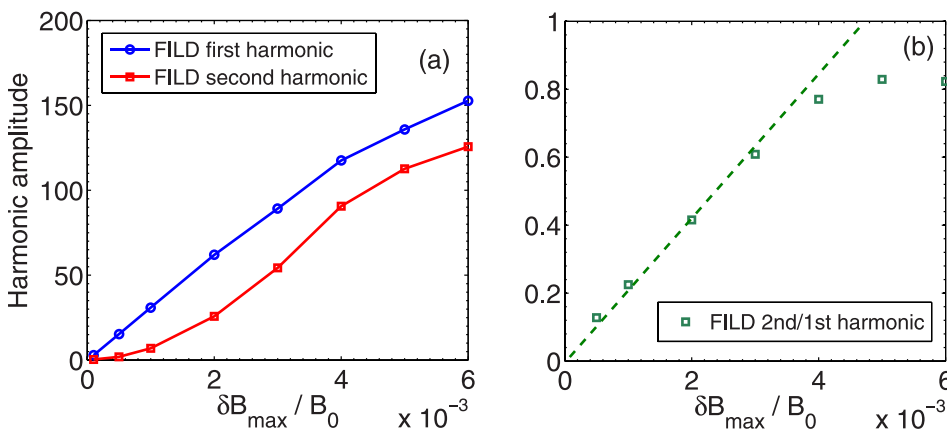

FIG. 14. FILD spectrum: (a) first and second harmonic amplitudes VS wave amplitude and (b) the ratio of the second harmonic over the first harmonic VS wave amplitude for the $q=q_{original}$ and $n=2$ RSAE case shown in Fig. 12(a).
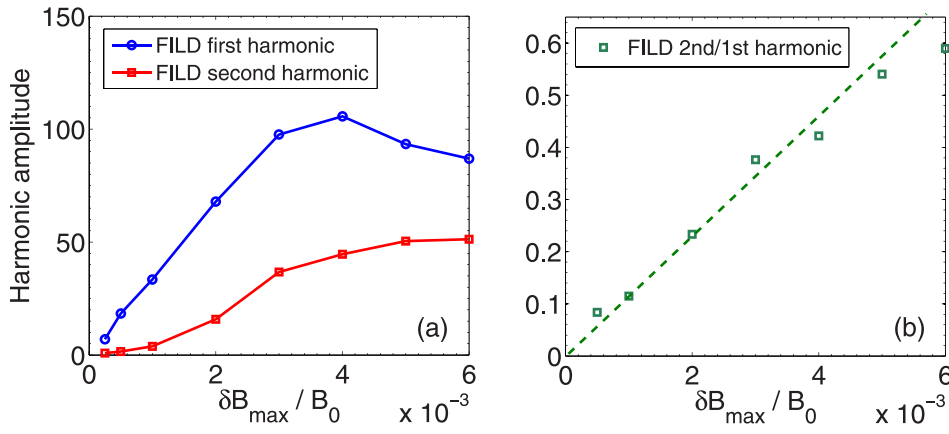
FIG. 15. FILD spectrum: (a) first and second harmonic amplitudes VS wave amplitude and (b) the ratio of the second harmonic over the first harmonic VS wave amplitude for AE modes shown in Fig. 13(a), $q_{min} = 3.28$ and $n = 3$ cases.
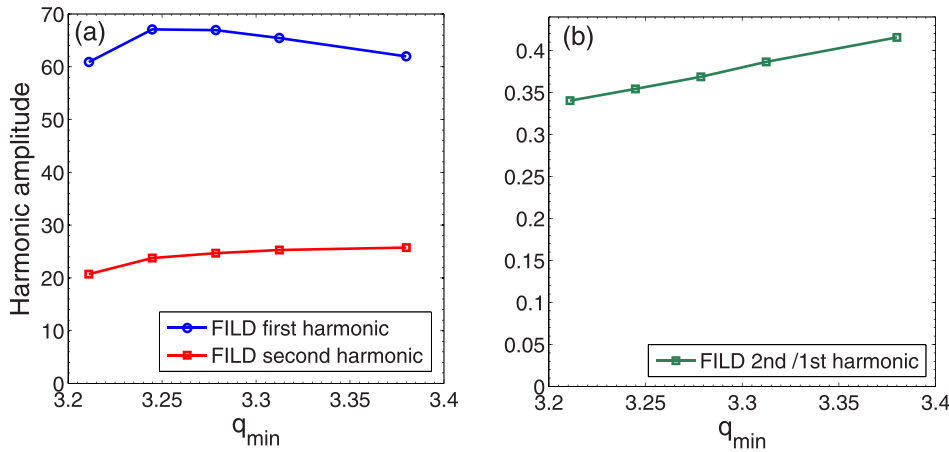

FIG. 16. (a) The first and second harmonic amplitude and (b) the ratio of the second harmonic over the first harmonic VS q value. The $n = 2$ mode structures and frequencies for different q values are shown in Fig. 12, where the amplitude given here is $B_{max}/B_0 = 0.002$.

Fig. 4. On the other hand, the sideband of the RSAE increases when q_{min} decreases as shown in Figs. 12 and 13, which may enhance the FILD signal. We believe that these two competing effects tend to cancel so that the FILD signal remains nearly constant as the mode changes.

It should be noted that the calculated ratios of second harmonics to the first harmonic based on the NOVA mode structure are about a factor of two larger than the corresponding results from the analytic n = 2 RSAE. This is because the NOVA mode structure [Fig. 12(a)] is wider and much complicated than the analytical mode [Eq. (2)]. Also, for the analytical AE mode, only the $m = 7$ mode, the most important poloidal harmonic, has been considered, while $m = 4$–8 modes have been retained in the NOVA results, which may lead to a stronger second harmonic. The ratios are a bit higher than the experimental observed values of less than 0.1 shown in Fig. 11 of Ref. 9. In their data base, the AE amplitude range is $\delta T_e/T_e = 0.005$–0.01 and $\delta B_{max}/B_0 = 0.001$ –0.002.

IV. MODE DRIVE DUE TO PROMPT LOSSES

In this section, we perform a realistic calculation of AE drive due to AE-induced prompt losses. The calculation is based on all prompt lost particles whether they are seen by FILD or not.

Figure 17 plots the time evolution of the net energy change of all lost particles with analytical AE perturbation given by Eq. (2) for several mode amplitudes. Note that the net energy change is negative for most of the time, but it is positive (energy gain) for some time even when the mode amplitude is large. This shows that not all the lost particles lose energy to the wave. This is because there are particles deposited deep in the loss region in Fig. 8. These particles would move inward radially for a certain mode phase but still remain in the loss cone and lose to the wall after one
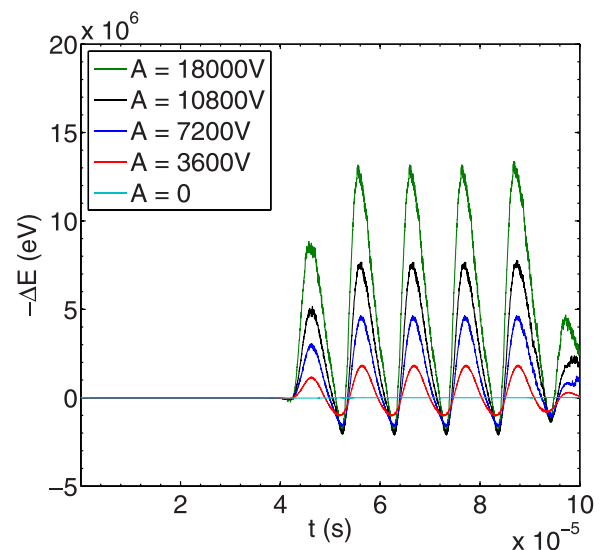

FIG. 17. Time evolution of the energy decrease for all loss particles. The $n = 2$ and $m = 7$ AE perturbation here is given analytically by Eq. (2), with frequency $f = f_0 = 96$ kHz.

bounce. The portion of these particles among all lost particles can be determined from Fig. 18, which plots energy change distribution for lost particles and confined particles for all particles injected over one wave period.

Figure 19 plots the time-averaged power loss fraction for all lost particles versus wave amplitude. The time range of the average is three wave periods as shown in Fig. 17. The loss fraction is defined as the ratio of the time-averaged particle energy loss over the total injected particle energy, i.e., the fraction of injection power to drive the AE mode. The averaged loss power fraction is quadratic in the wave amplitude for $\delta B_{max}/B_0 < 2.7 \times 10^{-3}$.

Following Heidbrink et al.,[11] the mode drive power or energy loss power can be calculated by

$$P_{drive} = f_{depo} f_E P_{inj}, \qquad (4)$$

where P_{inj} is the neutral beam injection power, which is 4.6 MW in DIII-D shot 146096, f_{depo} is the fraction of injected beam ions that are lost to the wall, and $f_E = \delta E/E_0$ is the averaged fraction of particle energy per lost particle that is delivered to the mode. For the case of Figs. 17, 18, and 19 with analytic n = 2 RSAE at $\delta B/B_0 \simeq 0.002$, $f_{depo} = 0.42\%$ and $f_E = 1.58\%$. Thus, we arrive at

$$P_{drive} = f_{depo} f_E P_{inj} = 0.0042 \times 0.0158 \times P_{inj} = 305 \text{ W}. \quad (5)$$

Using these numbers, the normalized mode drive can be obtained as

$$\frac{\gamma}{\omega} = \frac{P_{drive}}{2\omega E_{mode}} = 5.17 \times 10^{-5}, \qquad (6)$$

where $E_{mode} = 4.89$ J is the mode energy. We have also calculated the mode drive based on more realistic AE mode structures obtained from the NOVA code. For the case of the n = 2 RSAE with $q = q_{original}$ and $\delta B/B_0 \simeq 0.002 (\delta T_e/T_e \simeq 0.01)$, the results are $P_{drive} = 69.35$ W and $\gamma/\omega = 1.3 \times 10^{-5}$, which is even smaller because the wave frequency is

FIG. 19. Lost particles' averaged power loss fraction VS amplitude. The n = 2 and m = 7 AE perturbation here is given analytically in Eq. (2).

farther from the peak of local resonance frequency. Compared to the previous estimate of mode drive $\gamma/\omega = 4 \times 10^{-3}$,[11] our drive is much lower and can be ignored. The discrepancy mainly comes from the over-estimation of f_{depo} and f_E in the previous work. Specifically, our value of $f_{depo} = 0.42\%$ is about a factor of 5 smaller than the previous estimate of $f_{depo} = 2\%$ and our value of $f_E = 1.58\%$ is a factor of 8 smaller than the previous estimate of $f_E = 13\%$. The overestimation of f_{depo} in the previous work is partly due to the fact that some of the particles near the local resonance may not be lost promptly if they are first kicked inward by the AE. In the previous work,[11] the authors assumed that all particles near the boundary that satisfy the local resonance condition would be lost, irrespective of their initial phase relative to the wave. They assumed that these particles would continue to interact with the mode until they were lost. But, from Fig. 18, we find that the number of particles lost after two bounces ($\delta E/E_0 < -0.05$) is much smaller than the number lost in one bounce. The number of particles lost after multiple bounces is found to be negligible since they obey the regular resonance condition rather than the local one. The overestimation of f_E can be explained by the results in Fig. 18 (see blue curve) and Fig. 20. The 10 cm maximum radial displacement leading to 13% energy loss[11] may be overestimated for the high frequency mode shown in Fig. 20. In Fig. 18, it is shown that the energy change of lost particles has a wide distribution in the range of $-0.05 < \delta E/E_0 < 0.05$, i.e., some of the lost particles actually gain energy as explained above. Thus, the averaged energy loss per lost particle is smaller.

Finally, let us estimate the size of the radial kick of trapped particles due to the local resonant interaction with the AEs. Figure 20 plots the maximum radial displacement of 1000 trapped particles for two mode frequencies (52 kHz and 96 kHz). The particles are located at $R = 2.26$ m on the midplane with an initial pitch angle distribution similar to the experimental deposition for an entire wave period. The displacement is measured when a particle crosses the outer
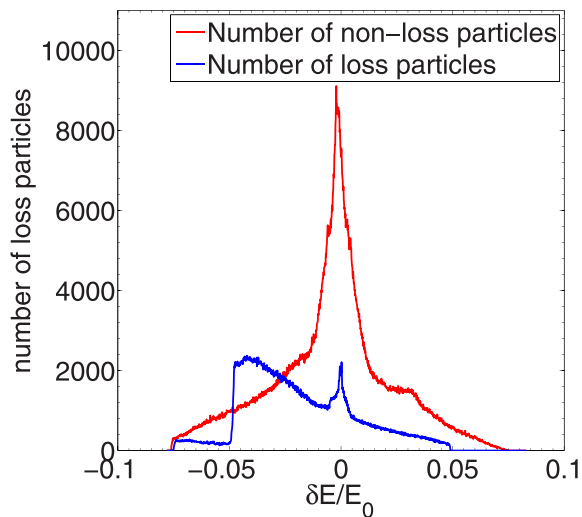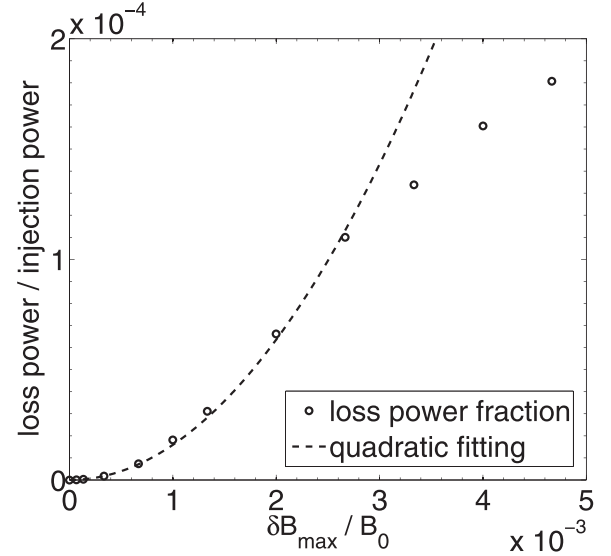

FIG. 18. Energy change distribution for loss particles and non-loss particles, where the energy grid is $10 \text{ eV}/E_0 = 1.24 \times 10^{-4}$ and particles are injected in one wave period. The analytical RSAE perturbation is given by Eq. (2), with $f = 96$ kHz, $A = 10\,800$, or $\delta B_{max}/B_0 \simeq 0.002$.
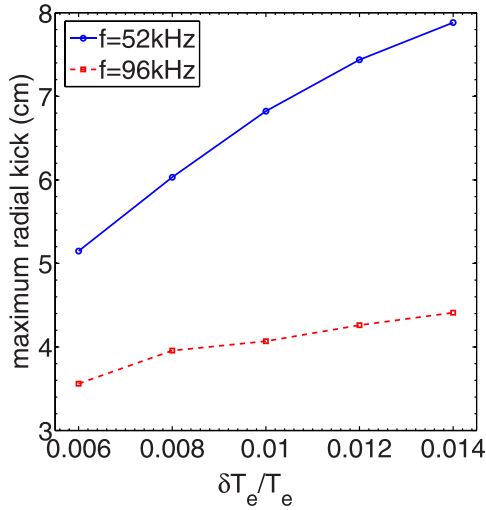
FIG. 20. Maximum radial displacement of 1000 trapped particles after one bounce VS $\delta T_e/T_e$.

midplane. We find that the maximum displacement for the $f = 52$ kHz AE is larger than that of the f = 96 kHz case. This is because the lower frequency is nearer the center of local wave particle resonance. The calculated radial kick size is comparable to the experimental values of 10 cm for the 52 kHz case,[6] but it is about 4 cm for the 96 kHz case, which is less than half of the experimental estimate.[11] As a result, the calculated energy loss per lost particle is smaller than that in the previous work.[11]

The calculated radial kick of 4 cm corresponds to the boundary in energy change $|\delta E/E| < 0.05$ as seen in Fig. 18. In previous work,[11] the larger experimental value of 10 cm kick size has been translated directly into $f_E = 0.13$. This means that a higher boundary of the $\delta E/E$ distribution has been assumed and the averaging over the $\delta E/E$ distribution has been neglected. These two effects combined explain the difference between the estimate of f_E in this work and Ref. 11.

V. CONCLUSION

In conclusion, a numerical study has been performed on the coherent beam ion prompt losses driven by Alfvén eigenmodes (AE) in DIII-D plasmas using realistic experimental parameters and beam ion deposition profiles. The synthetic signal of the fast-ion loss detector (FILD) is calculated for a single AE mode. The first harmonic of the calculated FILD signal is found to be linearly proportional to the AE amplitude with the same AE frequency in agreement with the analytic theory and the DIII-D experimental measurement. The calculated second harmonic is proportional to the square of the first harmonic for typical experimental AE amplitudes. The amplitude of the second harmonics of the FILD signal is found to scale quadratically with the first harmonic. The size of the second harmonic is found to be sensitive to the mode width. This result can explain partly poor

correlation of the second harmonic with the first harmonic. Future work will further explore the sensitivity of the second harmonic and more generally nonlinear harmonics in the presence of multiple modes. The second part of this work considers the AE drive due to coherent prompt losses. It is shown that the prompt-loss-induced mode drive is much smaller than the previous estimate and can be ignored for mode stability.

[1]M. Garcia-Munoz, N. Hicks, R. van Voornveld, I. G. J. Classen, R. Bilato, V. Bobkov, M. Brambilla, M. Bruedgam, H.-U. Fahrbach, V. Igochine, S. Jaemsae, M. Maraschek, K. Sassenberg, and ASDEX Upgrade Team, Nucl. Fusion **50**, 084004 (2010).
[2]K. Ogawa, M. Isobe, K. Toi, F. Watanabe, D. A. Spong, A. Shimizu, M. Osakabe, S. Ohdachi, S. Sakakibara, and LHD Experiment Group, Nucl. Fusion **50**(8), 084005 (2010).
[3]M. A. Van Zeeland, W. W. Heidbrink, R. K. Fisher, M. G. Munoz, G. J. Kramer, D. C. Pace, R. B. White, S. Aekaeslompolo, M. E. Austin, and J. E. Boom, Phys. Plasmas **18**, 056114 (2011).
[4]X. Chen, R. K. Fisher, D. C. Pace, M. Garcia-Munoz, J. A. Chavez, W. W. Heidbrink, and M. A. Van Zeeland, Rev. Sci. Instrum. **83**, 10D707 (2012).
[5]X. Chen, M. E. Austin, R. K. Fisher, W. W. Heidbrink, G. J. Kramer, R. Nazikian, D. C. Pace, C. C. Petty, and M. A. Van Zeeland, Phys. Rev. Lett. **110**, 065004 (2013).
[6]X. Chen, W. W. Heidbrink, G. J. Kramer, M. A. Van Zeeland, M. E. Austin, R. K. Fisher, R. Nazikian, D. C. Pace, and C. C. Petty, Nucl. Fusion **53**, 123019 (2013).
[7]X. Chen, W. W. Heidbrink, M. A. Van Zeeland, G. J. Kramer, D. C. Pace, C. C. Petty, M. E. Austin, R. K. Fisher, J. M. Hanson, R. Nazikian, and L. Zeng, Rev. Sci. Instrum. **85**, 11E701 (2014).
[8]X. Chen, G. J. Kramer, W. W. Heidbrink, R. K. Fisher, D. C. Pace, C. C. Petty, M. Podesta, and M. A. Van Zeeland, Nucl. Fusion **54**, 083005 (2014).
[9]W. W. Heidbrink, E. A. D. Persico, M. E. Austin, X. Chen, D. C. Pace, and M. A. Van Zeeland, Phys. Plasmas **23**, 022503 (2016).
[10]R. B. Zhang, G. Y. Fu, R. B. White, and X. G. Wang, Nucl. Fusion **55**, 122002 (2015).
[11]W. W. Heidbrink, G.-Y. Fu, and M. A. Van Zeeland, Phys. Plasmas **22**, 082507 (2015).
[12]R. J. Goldston, D. C. McCune, H. H. Towner, S. L. Davis, R. J. Hawryluk, and G. L. Schmidt, J. Comput. Phys. **43**, 61 (1981).
[13]J. Zhu, G. Y. Fu, and Z. W. Ma, Phys. Plasmas **20**, 072508 (2013).
[14]C. Z. Cheng and M. S. Chance, J. Comput. Phys. **71**, 124 (1987).
[15]R. B. White, *The Theory of Toroidally Confined Plasmas*, 2nd ed. (Imperial College Press, London, 2001).
[16]R. B. White, N. Gorelenkov, W. W. Heidbrink, and M. A. Van Zeeland, Phys. Plasmas **17**, 056107 (2010).
[17]Y. Kusama, H. Kimura, T. Ozeki, M. Saigusa, G. J. Kramer, T. Oikawa, S. Moriyama, M. Nemoto, T. Fujita, K. Tobita, G. Y. Fu, R. Nazikian, and C. Z. Cheng, Nucl. Fusion **38**, 1215 (1998).
[18]S. E. Sharapov, D. Testa, B. Alper, D. N. Borba, A. Fasoli, N. C. Hawkes, R. F. Heeter, M. Mantsinen, M. G. von Hellermann, and EFDA-JET Work-Programme, Phys. Lett. A **289**, 127 (2001).
[19]C. Z. Cheng, L. Chen, and M. Chance, Ann. Phys. **161**, 21 (1985).